Phase Transitions in the Anisotropic Ferrimagnetic Ytterbium Iron Garnet*

Richard Alben
Becton Center, Yale University, New Haven, Connecticut 06520
(Received 9 March 1970)

The thermal and magnetic properties of YbIG in field-induced canted configurations are discussed with emphasis on phase-transition singularities. By using the (for this case, well-justified) mean-field formalism of Wolf and the $\vec{G}$ and $\vec{g}$ tensors of Wickersheim, we calculate properties for applied fields of 0 to 300 kOe and for temperatures from 0 to 30 °K. Complete entropy and magnetic-moment predictions are presented for the field along the [111] and [100] directions. Selected results for specific heat and susceptibility are given for [111], [100], and [314] directions. We also discuss torque curves and variation of level splittings with applied field. Although it is clear that the Wickersheim parameters do not provide an over-all "best fit," the agreement for such data as are available is qualitatively good. Unfortunately, there are few data suitable for comparison with the phase-transition predictions. Four kinds of phase transitions are predicted: (I) ordinary first order, (II) liquid-vapor-like second order, (III) symmetry-affected first order, and (IV) symmetry-affected second order. Of particular interest are the following divergence and near divergence of the specific heat C for examples of the second and third types, respectively: (II) (T near $T_c = 7.51$ °K, $H = 43.640$ kOe along [100]) $C \sim 0.36(T-T_c)^{-2/3} R$/mole; (III) ($T < T_t = 16.18$ °K, $H = 110$ kOe along [111]) $C \sim 6.0 (1+\{3/[1-60(T-T_t)]^{1/2}\})R$/mole. A phenomenological theory applicable to all RIG's and perhaps other ferrimagnets describes very well the singularities in thermal-magnetic properties at the phase transitions and also the positions of phase boundaries.

I. INTRODUCTION

The sublattices of Néel ferrimagnets become noncollinear in large magnetic fields. This field-induced canted configuration,[1] though long known[2] (the spin-flopped state in an antiferromagnet[3–6] is a special case of it), has only recently been characterized for systems without anisotropy.[6] Some special cases including anisotropy have also been mentioned, but these either were restricted to antiferromagnets[5] or did not include a realistic treatment of the temperature variation of the moments.[7,8] In this paper we present a theory of ytterbium iron garnet $Yb_6Fe_{10}O_{24}$ in a (for this case quite credible) mean-field approximation including anisotropy and the influence of field and temperature on the six Yb sublattices. Emphasis is on the canted configurations which occur for temperatures T below about 17 °K and in applied field H of from 0–300 kOe.

In Sec. II we review the mean-field model of YbIG and describe our numerical methods for finding the lowest-energy sublattice configuration predicted by the model. In Sec. III we present results of calculations for physical properties of YbIG and compare, where possible, to reported measurements. We give complete curves for entropy S and moment M in the H-T plane for fields along [111] and [100] and also for M against T for selected fields and M against H for selected temperatures. Specific heat C and susceptibility χ and also torque-curve predictions are given as a function of temperature for selected fields. Doublet level splittings are presented as a function of field for the compensation temperature. By and large, agreement with experiment is satisfactory. However, since there are very few data taken in high fields, and essentially none for single crystals at high fields, the most interesting predictions, those for phase transitions, are largely untested.

In Sec. IV we develop an order-parameter description of the isotropic ferrimagnet. In analogy with the YbIG theory, the angle of one of the sublattices plays the role of the order parameter. The single type of phase transition, that between canted and aligned phases, is of second order; S and M are continuous; C and χ are discontinuous but finite.

In Sec. V we extend the description to include certain representations of anisotropy. Anisotropy multiplies the number of possible phases, and the transitions among them are classified into four types according to thermodynamic behavior: (I) ordinary first order (lines in the H-T plane) – S, M, C, and χ all discontinuous; (II) liquid-gas-like second-order isolated points – S and M continuous, C and χ diverge (except possibly along the coexistence curve); (III) symmetry-affected first-order lines – S and M discontinuous, C and χ rise steeply before a discontinuity; (IV) symmetry-affected second-order isolated points and lines – S and M continuous, C and χ discontinuous. The type of transition as well as the position of the phase boundaries depend sensitively on the applied-field

direction. These features are illustrated with cases from the YbIG calculation and are also described in terms of phenomenological concepts of rather more general applicability.

II. MEAN-FIELD CALCULATION FOR YbIG

Several detailed discussions of the interactions in YbIG have been published[9]; we present here only a brief review. The Fe^{3+} ions, located on a and d sites, are strongly internally coupled (500 °K), and, at low temperature, effectively form a single rigid saturated sublattice. The state of any given Fe^{3+} is that of the sublattice as a whole, the back reaction of neighboring Yb^{3+} ions being negligible. This justifies a mean-field approach to the Yb-Fe interactions.[10] The Yb ions, on six inequivalent c sites, interact negligibly among themselves and form a noncooperative "paramagnetic" system. The lowest Kramers doublet of Yb^{3+} in the c-site crystal field is well separated from other states, and with but subtle corrections[11] its spin Hamiltonian describes the behavior. Interactions within the ground doublet are given by exchange ($\underline{G}$) and paramagnetic ($\underline{g}$) tensors which have been measured to about 10% accuracy by various means and been found to be quite anisotropic.[12] The anisotropy of YbIG has its origin in these interactions. The Yb moment decreases with a characteristic temperature of about 20 °K, equivalent to the average Yb-Fe exchange energy.

Many features of the behavior of YbIG depend on a subtle cancellation between Yb and Fe magnetic moments. Measurements on a good sample[6] indicate that at 0 °K the Yb moment dominates the Fe moment by about $\frac{1}{2}$% (10.07 versus $10.00\beta/6$ Yb's).[13] There seems to be a compensation point at 7 °K. Clearly a 1% change in the assumed $\underline{g}$ tensor could eliminate the compensation point from a theoretical model, as a similar error in stoichiometry could eliminate it in a test sample. Thus, even within the experimental errors in $\underline{G}$ and $\underline{g}$, some judicious choosing is necessary. It happens that the parameters reported by Wickersheim[12] – $\underline{g}$ from EPR on Yb^{3+} in yttrium gallium garnet and $\underline{G}$ from near infrared on Yb^{3+} in YIG at 77 °K – reproduce closely the observed compensation point, and we have used them for the calculations.[14] These parameters are given in Table I.

Our calculation was a straightforward application of the theory of two-level paramagnetic ions in exchange and magnetic fields.[15] For a given temperature and magnitude and direction of external field, a series of guesses were made for the direction of the iron sublattice. Next, the effective fields at each of the six inequivalent Yb sites were determined via the $\underline{G}$ and $\underline{g}$ tensors and then the Yb-ion free energies were calculated.

TABLE I. Principal values of G and g tensors used in YbIG calculation (from Wickersheim, Ref. 11). G is from near-infrared measurements on YIG at 77 °K, and g is from paramagnetic resonance in Yb-doped YGaG.

Principal axis	G (cm^{-1})	g
x	11.6	2.85
y	25.7	3.60
z	29.9	3.78

This added to a small Fe sublattice anisotropy correction and the Fe Zeeman interaction gave the total free energy to be minimized against variation of the assumed Fe sublattice direction.

Letting the level splitting of a site on the ith Yb sublattice ($i = 1, 6$) be Δ^i we have

$$\Delta^i = \left| \beta \vec{H} \cdot \underline{g}^i - (\vec{M}_F / |M_F|) \cdot \underline{G}^i \right| , \tag{1}$$

where the principal axes of the $\underline{g}^i$ and $\underline{G}^i$ tensors are appropriate to the ith sublattice. The set of angles giving the direction of the Fe sublattice (i.e., $\vec{M}_F/|M_F|$) will be denoted Θ. The free energy as a function of Θ, H, and T is given by

$$F(\Theta, H, T) = -kT\textstyle\sum_i n^i \ln 2\cosh[\Delta^i(\Theta)/kT] - \vec{M}_F \cdot \vec{H} + A(\Theta) , \tag{2}$$

where n^i is the number of Yb's on the ith sublattice, one mole for each i in most of our calculations. The Fe sublattice anisotropy term A is quite small[16]; it is a K_1 cubic-type term with $K_1 = 2.4\times10^4$ erg/cm^3 or $0.08R$/mole 6 Yb's.

The two procedures used to find the lowest minimum of F are described below. We here note that, especially near phase transition, some care was required. With a minor exception,[17] however, for the cases reported in this paper, there is little doubt that the lowest minimum was found.

Procedure I: Minima were found for rotation angles in a given plane. This could be used only for fields applied along directions of high symmetry, for only then could all reasonable possibilities for the "easy plane" be examined. For fields along [111] and [100], the lowest minima occurred in the (110) plane. For a wide sampling of fields and temperatures it was verified that no lower minima occurs in either (110) or (112). The method converged satisfactorily to within several hundredths of a degree of most second-order transitions. (First-order transitions occur between well-defined local minima and present no particular difficulty.) Each minimum was tested for stability against small out-of-plane displacements.

Procedure II: A search was started at a given point on the energy surface and proceeded down the local free-energy gradient until a minimum was reached. Then a lower minimum was found

for angles along the perpendicular to the first search direction and so on until no further improvement could be achieved. The method was used for fields along nonsymmetry directions. For fields below 50 kOe, the local minima are well-defined and are all accessible from the eight [111] directions, the easy sublattice directions for zero field. Eight start points were used to generate the torque results given in Sec. III E. For higher fields the scheme tended to run wild whenever minima occurred close together, thus making the investigation of second-order transitions in the low-symmetry direction [314] very difficult. We used 16 start points in order to derive the [314] phase diagram (Sec. IV C) and physical properties (Sec. III C). We also ran checks on the [111] and [100] results from various start points and verified again that the lowest minimum is always for the Fe moment in the (110) plane.

Once the Fe sublattice direction was found, we calculated the various thermal and magnetic properties. For S and M we have

$$S = -\frac{\partial}{\partial T}\,\mathrm{F}(\Theta, H, T) - \frac{\partial}{\partial \Theta}\,\mathrm{F}(\Theta, H, T)\frac{\partial \Theta}{\partial T}$$
$$= -\frac{\partial}{\partial T}\,\mathrm{F}(\Theta, H, T)\,, \qquad (3)$$
$$M = -\frac{\partial \mathrm{F}}{\partial \vec{\mathrm{H}}} - \frac{\partial \mathrm{F}}{\partial \Theta}\frac{\partial \Theta}{\partial H} = -\frac{\partial \mathrm{F}}{\partial H}\,,$$

where the arguments of the free energy F have been supressed in the second equation. Since the analytic form of F as a function of H, T, and Θ is known, the derivatives on the right-hand side of Eq. (3) may be computed directly:

$$S = k\textstyle\sum_i n^i\left[-(\Delta^i/kT)\tanh\Delta^i/kT + \ln 2\cosh\Delta^i/kT\right],$$
$$\vec{\mathrm{M}} = \beta\textstyle\sum_i n^i \tfrac{1}{2}\tanh(\Delta^i/kT) \qquad (4)$$
$$\times\left[\beta\vec{\mathrm{H}}\cdot\underline{\mathrm{g}}^i\cdot\underline{\mathrm{g}}^i - (\vec{\mathrm{M}}_F/|M_F|)\cdot\underline{\mathrm{G}}^i\cdot\underline{\mathrm{g}}^i\right]/\Delta^i + \vec{\mathrm{M}}_F\,.$$

Furthermore, the torque is just $M\times H$.

The thermodynamic expressions for C and χ are

$$C = -T\frac{\partial^2}{\partial T^2}\,\mathrm{F} - T\frac{\partial^2 \mathrm{F}}{\partial\Theta\partial T}\frac{d}{dT}\,\Theta,$$
$$\chi = -\frac{\partial^2}{\partial H^2}\,\mathrm{F} - \frac{\partial^2 \mathrm{F}}{\partial\Theta\partial H}\frac{d}{dH}\,\Theta\,. \qquad (5)$$

The functional form of Θ is not known in our work, so unlike S and M, C and χ require numerical differentiation for their computation. For the results reported in this paper, there is no significant numerical error in this procedure except within 0.2 °K of second-order phase transitions. Even then the error is unresolvable in results presented as graphs. However, this error is sufficiently large so that the analytical form of the singular thermodynamic function could not be accurately found from numerical results alone. Our results for critical exponents, etc., thus rely heavily on knowledge of the analytical properties of $\mathrm{F}(\Theta, H, T)$.

III. PREDICTED PROPERTIES OF YbIG

Most physical properties of the canted phases of YbIG are qualitatively similar to those of an isotropic ferrimagnet. (See Ref. 6 and also our reformulation of Sec. IV). The principal difference is that in YbIG there occur anisotropy-associated phase-transition singularities. The nature and location (in H-T) of the transitions depend strongly on field direction. Below, we present results for what is necessarily a limited number of field directions. The properties discussed are entropy, moment, specific-heat, susceptibility torque, and level splittings. Where possible, experimental results are included for comparison

A. Entropy

In Figs. 1 and 2, we present computed isentropes for a range of field (along [111] and [100]) and temperature which includes the entire canted region. Isentropes represent trajectories traced by a thermally insulated sample in a variable field. Agreement with the experiment[18] on a polycrystal is qualitatively good. The lower slope and higher transition temperature of the experimental result indicate that the exchange splittings in the actual material are, on the average, higher than those used in the model. In other words, the relative insensitivity (of the actual material) to changes in temperature indicates a larger separation in the actual ground doublets than in those of the model.

B. Magnetic Moment

In some sense all thermodynamic information is contained in the functions $S(H, T)$ and $M(H, T)$; so, to complement the isentropes, we present, in Figs. 3 and 4, lines of constant moment for H along [111] and [100], respectively. Some of the same information, in more familar form, is given in Figs. 5 and 6 where we present M-versus-T curves. M is far from constant in the canted phase, large drops occurring at phase transitions (M would be temperature independent if anisotropy were neglected). The experimental points (for [111]) of Clark[19] seem to show these discontinuities. The lower slope and higher transition temperature of the experimental data again indicate that a higher average exchange is operative. M against H for [111] is shown in Fig. 7.[20]

C. Specific Heat

Figure 8 shows computed specific heat in zero

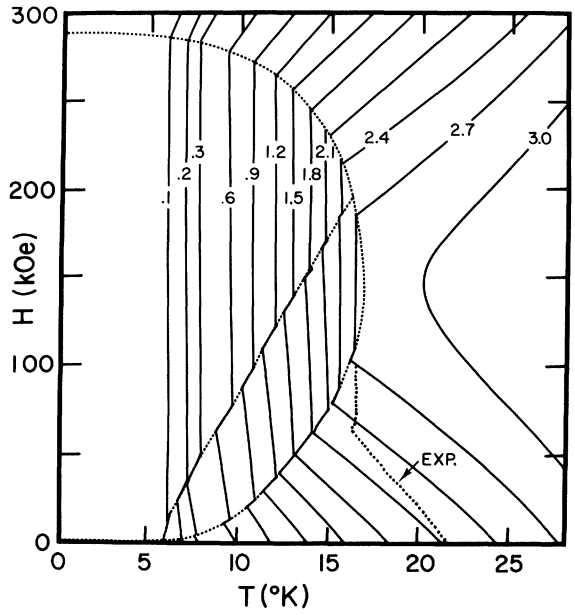

FIG. 1. Isentropes for H along [111]. Labels are in cm^{-1} units, divide by 0.695 for R/mole. A lattice contribution (Ref. 27) is included. The jags occur at first-order phase boundaries (indicated where possible by square dots). Horizontal separation of isentropes is inversely proportional to C/T. Note the increase of latent heats from zero at $H=0$ to a maximum at about 80 kOe followed by a decrease as the second-order point at 197 kOe is approached. Also the isentropes are not strictly vertical in the canted phase, but have negative slopes between phase transitions. This is because anisotropy partially pins the R sublattice, and applied field can then cancel exchange somewhat as H is increased. (In the isotropic case, h^{eff} and, thus, S is H independent in the canted phase.) An experimental isentrope (small dots) of Clark (Ref. 18) measured on a polycrystal is included for comparison. Note the jag as some crystallites undergo a first-order transition to the canted phase. Dashed lines are phase boundaries.

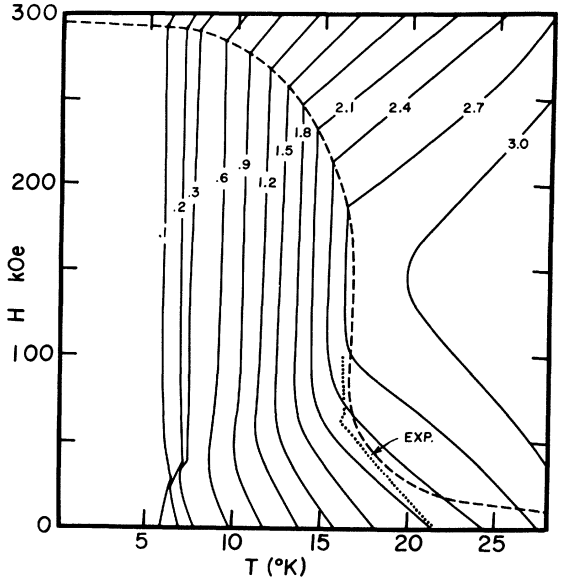

FIG. 2. Isentropes for H along [100]. Note the break in slope at second-order phase boundary (dashed lines). Also note that the 0.6 isentrope displays in a nonsingular way the same general trend characteristic of isentropes which cross the (expired) first-order transition. Clark's (Ref. 6) polycrystal isentrope is again indicated by the small dots.

field[21] compared to experimental points of Harris and Meyer.[12] The theoretical Yb Schottky anomaly occurs at too low a temperature, indicating once again that our exchange splittings are too low. In Fig. 9, we show specific heat for $H=100$ kOe along easy and hard directions. The [111] results show two first-order transitions, the second of which is symmetry affected (see Sec. V). For the field along [100] there is a single second-order transition. For reference, note that an isotropic model (see Sec. IV) would show C rising approximately as T^2 above about 10 °K to a maximum of $9(T_0/T_c)^2R$/mole, where T_0 is the transition temperature. In 100 kOe, this implies a maximum of about $7R$ occurring at 15 °K, whereupon there would be a sharp drop to paramagnetic behavior. Figure 10 shows results of 90 kOe for H along a nonsymmetry direction [314]. There are four first-order transitions whose latent heats together account for an

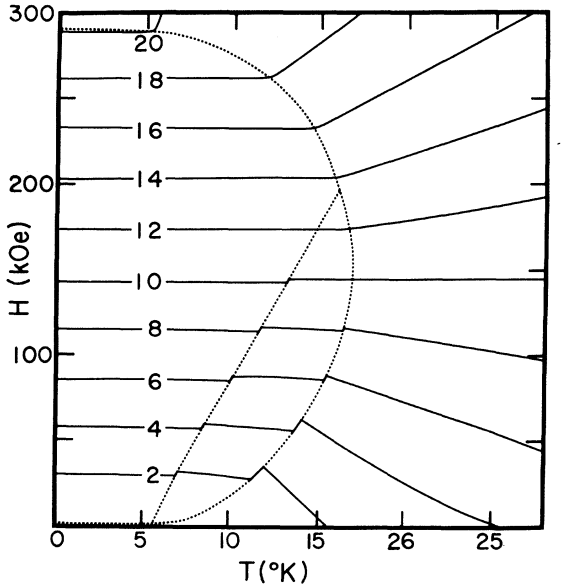

FIG. 3. Lines of constant moment for H along [111]. Labels are in $\beta/6$ Yb sites; multiply by 20 for emu/cm^3. Since S increases somewhat with H in the canted phase between transitions, M increases slightly with T. At transitions for which the boundary has positive slope, the high-T phase has the lower moment.

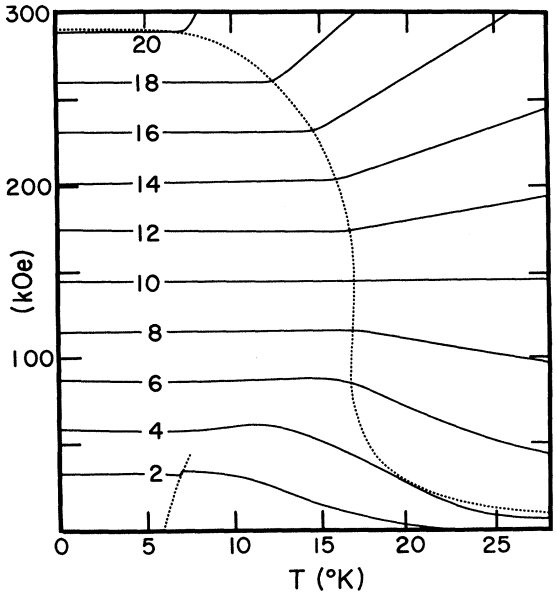

FIG. 4. Lines of constant moment for H along [111]. Note the break in slope at the second-order boundary.

entropy of $0.45R$, out of the maximum Yb contribution of $4.16R$.

D. Susceptibility

The magnetic susceptibility for three fields along [111] is shown in Fig. 11. In the canted phase, χ is roughly $1/\lambda$ or 1.3×10^{-3}. (See Sec. IV.) In the (high-temperature) aligned phase χ is a function of $|H-\lambda M_F|/T$ as for a paramagnet in an effective field.

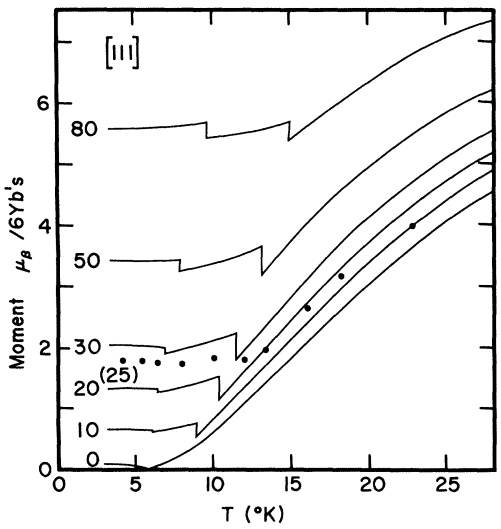

FIG. 5. M versus T for H along [111]. Labels are H in kOe. Points are experimental measurements of Clark and McGuire (Ref. 19) for 25 kOe.

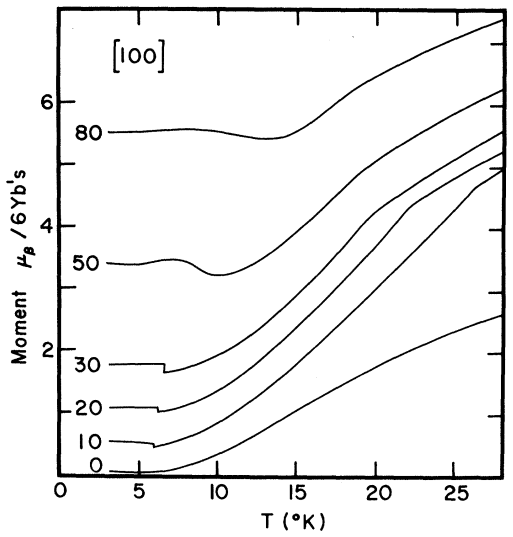

FIG. 6. M versus T for H along [100]. The first-order transition present for low field is not present above 44 kOe, but the general behavior of increase-decrease-increase of M with T is followed in a nonsingular fashion at H=kOe.

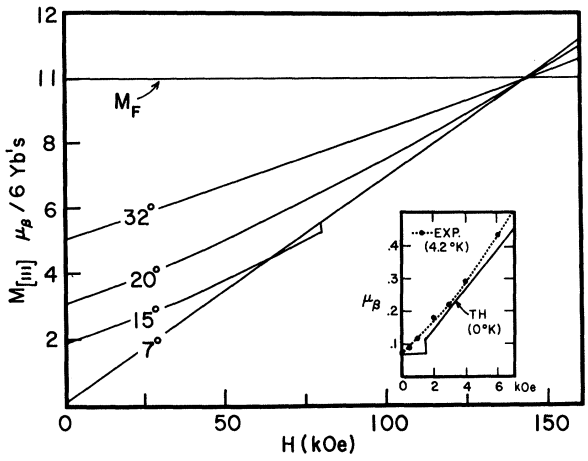

FIG. 7. M versus H along [111]. Labels are temperature in °K. The 7° line enters the canted phase at 1.5 kOe, the 15° line at 80 kOe. In the canted phase the lines are indistinguishable, reflecting the fact that M is almost T independent in the canted phase. Other lines represent essentially paramagnetic behavior, with the M_F line being the limit for high temperature. The lines do not precisely converge at H=145 kOe as they would for a two-sublattice isotropic model. The insert shows 0 °K theory compared to the 4.2 °K data of Clark (Ref. 6). The precise agreement at zero field is fortuitous, but the deviation of the experimental points from linearity is probably associated with an inhomogeneity-broadened transition to the aligned phase. This transition is sharp for the theoretical line.

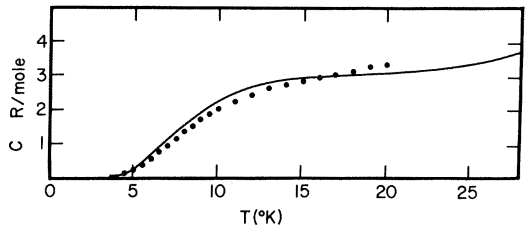

FIG. 8. Specific heat in zero field. A lattice background is included (see Ref. 21). Experimental points (circles) are from Harris and Meyer, Ref. 12. See also Ref. 21.

E. Torque

Whereas previously discussed properties of YbIG share many features with isotropic systems, torque owes its entire existence to anisotropy. Theoretical torque curves and a comparison with the data[22] of Schelleng and Clark are given in Fig. 12. The principal features of the low-temperature theoretical results are the transitions to different phases whenever we cross planes which bisect the "source" [111] directions (i.e., directions to which R would return if H were reduced to zero). For example, at 3 °K the R sublattice goes from $[-1-11]$ to $[11-1]$ when H rotates past [112] and then to $[1-11]$ when H passes [111]. The first two phases are "in plane," i.e., all moments in $(1-10)$, and the third is "out of plane." This and almost all low-temperature torque behavior can be understood from a simple phenomenological model.

We assume that anisotropy pins the sublattice near [111] directions so that the zero-field moment is along some [111], and the susceptibility along this [111] is quite small (since both sublattices are already aligned). The perpendicular susceptibility will be $1/\lambda$, assuming exchange dominates. Taking α as the angle between H and a particular [111] direction, we have

$$F = -HM_0\cos\alpha - \tfrac{1}{2}H^2(\chi_\perp - \chi_\parallel)\sin^2\alpha - \tfrac{1}{2}H^2\chi_\parallel , \quad (6)$$

where M_0 is the zero-field net moment. Letting $\chi_\perp - \chi_\parallel = \Delta\chi$ (the difference between parallel and perpendicular susceptibilities) we have for the torque

$$T = -HM_0\sin\alpha + H^2\Delta\chi\sin\alpha\cos\alpha . \quad (7)$$

The easy direction is gotten by minimizing Eq. (6)

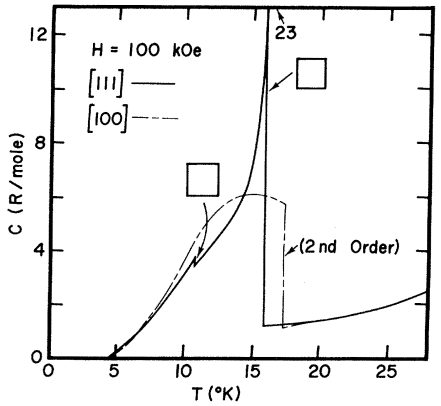

FIG. 9. Specific heat in 100 kOe for H along [111] and [100]. The squares represent by their areas the latent heats at the first-order transitions which occur for H along [111]. There is no latent heat for the second-order transition with H along [100].

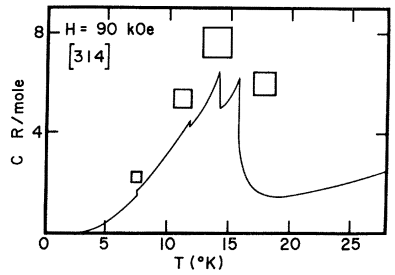

FIG. 10. Specific heat in 90 kOe for H along [314]. There are four first-order transitions (see Fig. 19). The tail at high temperature occurs because there is no abrupt transition to a completely aligned phase, but rather a continuous sublattice adjustment which persists to relatively high temperature.

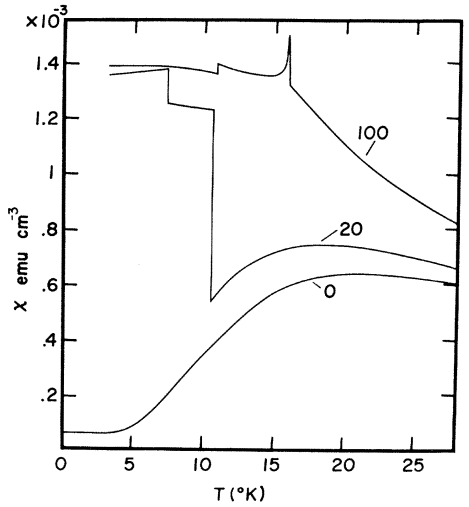

FIG. 11. Magnetic susceptibility for H along [111]. The zero-field predictions do not vanish as $T \to 0$ because of the Van Vleck temperature-independent susceptibility of the Yb sublattices, none of which are completely aligned along [111]. χ is about 1.3×10^{-3} in canted states except for phase-transition singularities. The sharp peak for $H = 100$ kOe is due to the symmetry-affected nature of the transition to the aligned phase (see Sec. V).

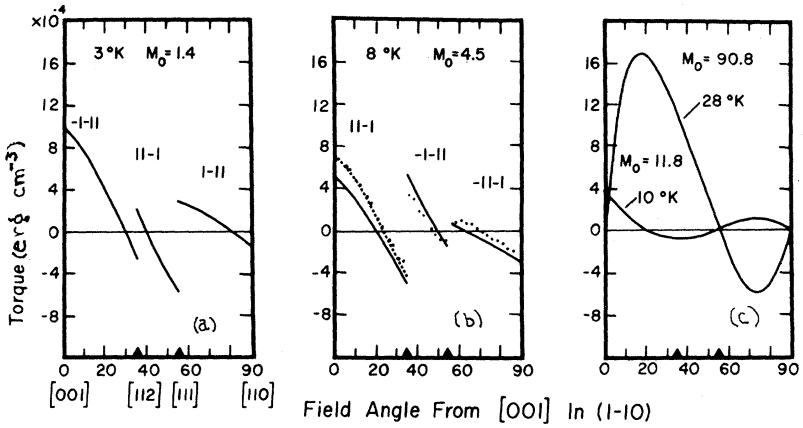

FIG. 12. Torque curves in (1-10) for $H=14$ kOe. Only the projection of the torque on [1-10] is given. The character of the predictions depends largely on the zero-field magnetic moment, so this is indicated for each temperature. (a) For 3 °K (below the compensation point) the phases go from $-1-11$ to $11-1$ to $1-11$ as the field is rotated. The effective torque in the $1-11$ (out-of-plane) phase is reduced because it is not paralled to $[1-10]$. (b) For 8 °K (above T_{comp}) the order is $11-1$, $-1-11$, $-11-1$ as indicated. Dots are experimental points of Schelleng and Clark (Ref. 22). The square dots give results of the phenomenological theory described in the text. (c) For 10 °K there is a phase transition at the [001] direction; the phase is -1 -1 -1 for the 0–90° quadrant. Note that here [111] is a hard direction. For 28 °K the sublattices are no longer pinned and there are no phase transitions (compare with Ref. 23).

with respect to α:

$$\alpha_{easy}=\cos^{-1}M_0/\Delta\chi H \quad \text{for } \Delta\chi H>M_0\,,$$
$$\alpha_{easy}=0, \qquad \text{otherwise.} \tag{8}$$

When M_0 is large or the field is small, the sample turns so that H is near [111], thus taking advantage of the M_0H term in the free energy. For small M_0 or large H, the induced moment counts more heavily, so the sample turns so H is perpendicular to [111] to take advantage of the large $\chi_\perp$.

Flipping between phases occurs because for a fixed crystal direction the sublattices have a choice of [111]'s.

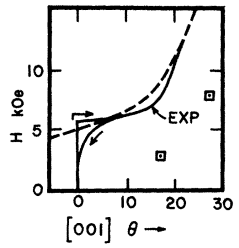

FIG. 13. Easy direction versus H. Experimental curve is from Ref. 22. The phenomenological theory (dashed curve) is $\theta=\cos^{-1}(M_0/\Delta\chi H)-54.7°$, where M_0 taken as 3.3 and $\Delta\chi$ is 1.2×10^{-3}. The two square points are for the six-sublattice model at 4.2 °K and are included only for general interest. We believe the six-sublattice calculation would fit the measured results, provided that M_0 (the zero-field moment) was adjusted to the experimental value. This adjustment could be accomplished well within the uncertainty of the parametrization of the theory.

In Fig. 12(b), we have plotted the prediction from Eq. (7) (phenomenological theory – dashed line) with $M_0=3.3$ and $\Delta\chi=1.2\times10^{-3}$ to obtain an essentially perfect fit to experiment. The numerically solved model (solid line) would have the proper value of M_0 for T somewhat less than 8° which is why we have compared the experimental points (taken at 4.2 °) with the 8° plot. Presumably, essentially perfect agreement for the six-sublattice model could be achieved if we made M_0 exactly equal to 3.3. Note that it is not possible to tell from the torque curves which sublattice has the larger moment.

In Fig. 13, we compare the predictions of Eq. (8) with the measured angle assumed by a freely rotating crystal (Ref. 22). The agreement with experiment is good except at very weak fields. Since the torque for a small displacement from the easy direction varies as H^2, we suspect that at these weak fields small mechanical irregularities might be impeding the rotation.

We see that torque measurements in the canted region are not particularly sensitive to the size of the anisotropy. The results in aligned or nearly aligned phases on the other hand do, of course, depend on anisotropy. Such a typical curve is shown in Fig. 12(c). Experimental results on torque in almost uncanted phases have been reported by Pearson[23] along with extensive theoretical discussion to which the reader is referred. We note here only that the parameters used in this model seem to predict torques about 20% too low at low temperatures and too high at high temperatures. (Experimental results on low-temperature aligned phases were obtained with samples diluted

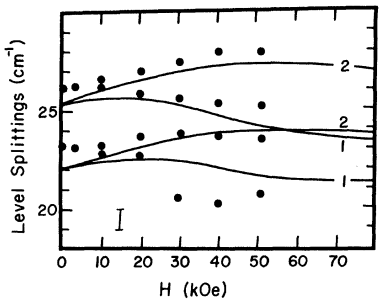

FIG. 14. Variation of exchange splittings with applied field along [111]. The experimental points are from Buchanan and Clark (Ref. 24). The estimated experimental error is 1 cm^{-1}, indicated at the lower left. The numbers at the right indicate the number of sites in the six-Yb cell which have the splitting given by the associated theoretical line. Were there no canting, there would be only two distinct splittings and these would decrease in magnitude at a rate of about 1.7 cm^{-1} per 10^4 Oe.

with yttrium.)

F. Exchange Splittings

Far-infrared measurements of exchange splittage of Yb^{3+} ions in YbIG in applied fields up to 51 kOe along [111] have been reported by Buchanan and Clark.[24] The transitions to canted configurations are clearly evidenced by the complete disagreement of these data with predictions derived for the Fe sublattice taken collinear with the field. On Fig. 14 we reproduce the 7.6 °K data reported in Ref. 24 and compare them to our predictions for 7 °K. Since the temperature is close to the compensation point, the canted phase is entered below 10 kOe. For higher fields, the results are not very sensitive to the degree of compensation. As with previous comparisons, the indication here is that the qualitative behavior of the predictions is generally correct, but the actual exchange splittings are higher than those predicted.

This completes the discussion of thermal and magnetic properties of YbIG *per se*. In Sec. V, however, we present further Yb results to illustrate behavior near the various types of phase transitions expected in all anisotropic ferrimagnets.

IV. PHENOMENOLOGICAL THEORY OF ISOTROPIC FERRIMAGNET

A. General Theory

We next reconsider (see Refs. 6 and 8) the isotropic two-sublattice ferrimagnet in terms of an "order-parameter" theory.[8,25] We constrain one sublattice F to point at a given declination angle θ_F to the external field H, where θ_F will be our order parameter. The other sublattice R finds its equilibrium consistent with θ_F. Anticipating the YbIG case, we take M_F (the moment of F) to be temperature and field independent. $M_R^{(T)}$ is, in the spirit of our mean-field approximation,[26] $M_R \times B_S(g\beta S h^{\rm eff}/kT)$, where, here, M_R means the $T = 0$ °K moment of R, $h^{\rm eff}$ is the effective field on M_R, B_S is the Brillouin function for spin S, g is the paramagnetic g factor, and β is the Bohr magneton. The free energy of the isotropic ferrimagnet with θ_F constrained to a set value is then

$$F^{\rm iso} = -\frac{kT}{g\beta S}\int_0^{g\beta S h^{\rm eff}/kT} M_R(y)\,dy - HM_F X_F + \bar{F}(T),$$

where

$$h^{\rm eff} = (H^2 + \lambda^2 M_F - 2\lambda H M_F X_F)^{1/2}\,, \quad X_F = \cos\theta_F\,. \tag{9}$$

λ is the antiferromagnetic F-R exchange constant, and $\bar{F}(T)$ is a nonmagnetic background.[27] Since everything in (9) is an explicit function of θ_F only, the problem has at this stage been reduced to finding the state of the F sublattice.

The unconstrained value of X_F (and thus θ_F) is found by minimizing Eq. (9). Thus,

$$X_F^{\rm iso} = (H^2 + \lambda^2 M_F^2 - \lambda^2 M_R^2)/2\lambda H M_F \quad \text{for} \quad |X_F^{\rm iso}| < 1 \tag{10a}$$

$$X_F^{\rm iso} = \pm 1, \text{ otherwise [sign is that of Eq. (10a)].} \tag{10b}$$

Equation (10a) applies for the canted state; (10b) is for the aligned state. For convenience later we call the minimum with respect to θ_F of applied field and exchange free energies the "exchange minimum." Since these parts of the energy depend only on θ_F and not on azimuthal angle ϕ_F, the exchange minimum is actually a ringlike depression on the energy surface. The curvature at $X_F^{\rm iso}$ is

$$\frac{\partial^2}{\partial X_F^2} F^{\rm iso}\bigg|_{X_F = X_F^{\rm iso}} = \frac{H^2 M_F^2}{\lambda M_R^2}\,. \tag{11}$$

Clearly, the exchange minimum is shallow at small fields, relatively steep when $H > \lambda M_R^2/M_F$. (An anisotropy field at right angles to H gives a minimum with curvature MH_a.)

In this approach we have concentrated on the F sublattice; θ_F was the order parameter. Note that it would have been awkward to pursue an exact solution using θ_R since M_R (magnitude) and, hence, the entire free energy is an exceedingly complicated function of θ_R. Single-sublattice anisotropy of the R sublattice, on the other hand, is most easily treated from an R point of view, and this will lead us to use simplifications of Eq. (9) in order to understand the exchange minimum in θ_R. The location of the R exchange minimum is, however, straightforward from knowledge of $X_F^{\rm iso}$:

$$X_R^{\rm iso} = (H^2 + \lambda^2 M_R^2 - \lambda^2 M_F^2)/2\lambda H M_R, \quad |X_R^{\rm iso}| < 1 \tag{12a}$$

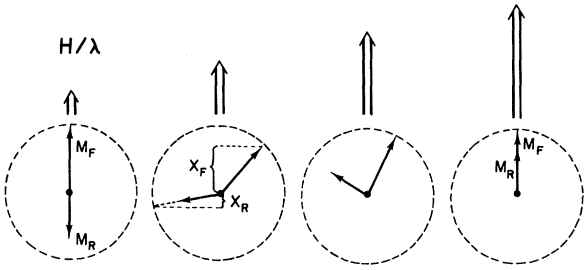

FIG. 15. Sublattice canting in the isotropic ferrimagnet at fixed T. $M_R^{(T)}$ is taken as less than M_F. For $H/\lambda < |M_F - M_R|$ the sublattices are antiparallel to minimize exchange. For $|M_F + M_R| > H/\lambda > |M_F - M_R|$ the best compromise of exchange and Zeeman energies is achieved by a canted state. For $H/\lambda > |M_F + M_R|$, the Zeeman energy dominates completely; M_R and M_F are parallel. X_F and X_R are direction cosines of F and R to the applied field direction.

$$X_R^{\text{iso}} = \pm 1, \text{otherwise [sign is that of Eq. (12a)]}. \tag{12b}$$

The general behavior of both sublattices is indicated schematically in Fig. 15 for three fields at a constant temperature where $M_F > M_R$. The sublattices start antiparallel. At larger field they enter the canted state. Finally, they become parallel when H is large enough to overcome the exchange. In Figs. 16 and 17 we show lines of constant X_F^{iso} and X_R^{iso} in the H-M_R plane. Since M_R decreases monotonically with temperature, the abscissa represents a scaled temperature with T increasing to the right. With our solution X_F^{iso} we may now return to Eq. (9) and evaluate S, M, C, and χ, according to Eqs. (3) and (5).

First note that the value of h^{eff} for $X_F = X_F^{\text{iso}}$ is particularly simple for the canted state:

$$h^{\text{eff}}(X_F^{\text{iso}}) = \lambda M_R(h^{\text{eff}}, T) . \tag{13}$$

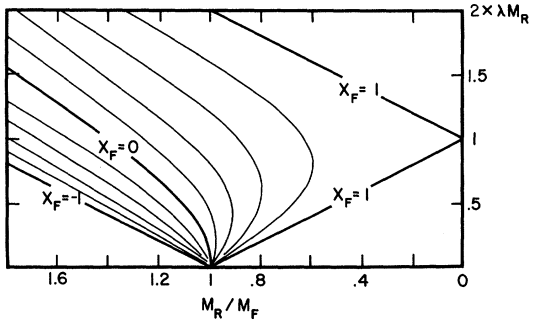

FIG. 16. Canting-angle direction cosine for F sublattice (isotropic ferrimagnet). M_R/M_F is a decreasing function of temperature for the Yb case, so the abscissa may be regarded as a scaled temperature for most purposes.

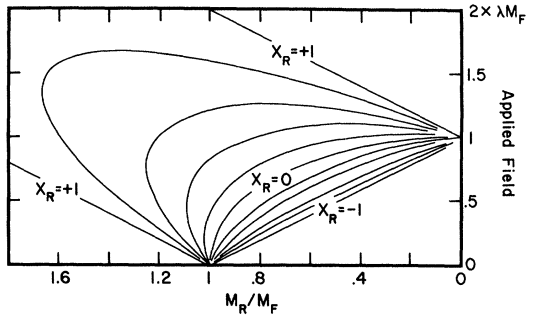

FIG. 17. Canting-angle direction cosine for R sublattice. The direction cosine X_R is indeterminate at the compensation point ($H=0$, $M_R/M_F=1$) and $M_R=0$.

Thus, M_R behaves much like an internally coupled ferromagnet with exchange constant λ:

$$M_R(T) = \bar{M}_R(T/T_c),$$

where

$$T_c = \lambda M_R g\beta(S+1)/3k, \tag{14}$$

and where M_R is the $T=0$ moment of R and $\bar{M}_R$ is the self-consistent solution to

$$\bar{M}_R(T/T_c) = M_R B_S(g\beta S\lambda \bar{M}_R/kT) . \tag{15}$$

Near $T = T_c$ we have (for $S = \frac{1}{2}$)

$$\bar{M}_R(T/T_c) \approx \sqrt{3} M_R(1 - T/T_c)^{1/2} T/T_c . \tag{16}$$

The above is valid only in the canted state. For the uncanted state the behavior is paramagnetic [see Eq. (17)].

The behaviors of S, M, C, and χ for the isotropic ferrimagnet are summarized in Table II. Note the following interesting features of the canted state: S is independent of H, M is independent of T, C is that for a ferromagnet of R spins with exchange constant λ, χ is independent of both T and H. In the aligned phases, the behavior is that of independent R spins in an effective field given by

$$h^{\text{eff}} = |H \pm \lambda M_F| , \tag{17}$$

where the plus applies when F is along H, the minus when it is opposed.

There is one phase transition for the isotropic ferrimagnet, a second-order line in the H-T plane separating aligned and canted phases. We consider the region where the Brillouin function for $S = \frac{1}{2}$ can be approximated by

$$B_{1/2}(y) \approx y - \tfrac{1}{3}y^3 . \tag{18}$$

Expanding (9) about $\theta_F = 0$ and keeping terms to fourth order we obtain

$$\begin{aligned} F^{\text{iso}} &= -(\theta_F^2/2!)F_x + (\theta_F^4/4!)(F_x + 3F_{xx}) , \\ F_x &= M_F H[T_c/T - 1 - (T_c/T)^3(\lambda M_F - H)^2/\lambda^2 M_R^2] , \\ F_{xx} &= \tfrac{2}{3} M_F H(T_c/T)^3(H/\lambda M_R)^2 . \end{aligned} \tag{19}$$

TABLE II. Summary of thermal and magnetic properties for an isotropic ferrimagnet. The F sublattice is taken as saturated. The R sublattice is made up of effectively paramagnetic spins of spin S and g-factor g is an exchange field λM_F and an external magnetic field H. Nonmagnetic contributions are neglected.

General relations	Canted phase	Aligned phase
$S=\frac{\partial F^{iso}}{\partial T}=\frac{-k}{g\beta S}\left[\int_0^y M_R\,dy'-M_R y\right]$	$y=\frac{g\beta S\lambda\bar{M}_R}{kT}$	$y=\frac{g\beta S\lvert\lambda M_F\pm H\rvert}{kT}$
$S(y=0)-S(y=\infty)=6\ln 2\,R/(\text{mole of } 6R \text{ spins})$		
$M=-\frac{\partial}{\partial H}F^{iso}=M_R\frac{H-\lambda M_F X^{iso}}{\lambda M_R}+X_F{}^{iso}M_F$	$\frac{H}{\lambda}$	$\lvert M_F\pm M_R\rvert$
$C=-T\frac{\partial^2 F^{iso}}{\partial T^2}-\frac{T\partial^2 F^{iso}}{\partial T\partial\theta_F}\frac{\partial\theta_F}{\partial T}-h^{eff}\frac{\partial M_R}{\partial T}$	$h^{eff}=\lambda\bar{M}_R$	$h^{eff}=\lvert\lambda M_F\pm H\rvert$
$\chi=-\frac{\partial^2 F^{iso}}{\partial H^2}\quad\frac{\partial^2 F^{iso}}{\partial H\,\partial\theta_F}\quad\frac{\partial\theta_F}{\partial H}$	$\frac{1}{\lambda}$	$\frac{\partial M_R}{\partial H}$

The aligned state becomes favored when F_x goes from positive to negative. The maximum temperature at which the canted phase can exist is thus T_c, this occuring when $H=\lambda M_F$. For higher or lower fields the transition occurs at a lower temperature. The curvature of the phase boundary at T_c is such that $\Delta T/T\sim(\Delta H/\lambda M_R)^2$. As may be discerned from Table II, S and M are continuous while χ and C have finite discontinuities across the transition.

B. Application to YbIG

For comparison with our anisotropic YbIG model, we note some general features of an isotropic analogy to YbIG. Following Clark[6] we make the following identification of parameters:

$$\begin{aligned} &M_F=200\ \text{emu/cc}\\ &\quad(\text{from measured density and taking } g_F=2)\ ,\\ &\bar{g}_R=3.4\ (\text{from averaging } g\text{'s in Table I})\ ,\\ &M_R=204\ \text{emu/cc}\ (\text{from } \bar{g}_R)\ ,\\ &\lambda=700\ (\text{from } \lambda M_F\beta\bar{g}_R=\text{average } G \text{ in Table I})\ . \end{aligned} \tag{20}$$

Then, from (5b) we have that $T_c=16.3\,^\circ$K. From Eq. (10), the highest field for which the canted state is possible is 280 kOe. From Table II, the susceptibility in the canted state is 1.4×10^{-3} emu/cc. Finally, the specific-heat discontinuity for $T=T_c$, $H=\lambda M_F$ is $\frac{3}{2}R/(\text{mole of spins})=9R/(6\text{ moles Yb})$. This last result is independent of λ, M, and g (see Ref. 26).

V. PHASE TRANSITIONS IN ANISOTROPIC FERRIMAGNET

A. Phenomenological Description

In this section, we address ourselves to the general nature of anisotropic ferrimagnets and their phase transitions. To the isotropic exchange and Zeeman energies we add a free energy which depends on the orientation of the crystal axes with respect to the sublattice magnetizations. In a two-sublattice ferrimagnet the anisotropy might appear in single-sublattice terms originating from either F or R or both, or as an anisotropic part of the exchange interaction.

Single-sublattice anisotropy can be described by a set of "anisotropy wells" in the free-energy surface at sublattice easy directions. The sum of the well and the exchange-minimum contributions to F then determines the effective easy direction for the sublattice as in Eq. (9). An example of a well contribution appropriate to a cubic crystal with H along [100] and where the azimuthal angle is fixed by taking (110) as the easy plane and where [111]'s are the easy directions is

$$F^{well}=A(T)(X^2-\tfrac{1}{3})^2\ , \tag{21}$$

where $A(T)$ is the anisotropy constant,[28] and X may refer to either F or R direction cosines to [100]. Anisotropy keyed to F, a temperature-insensitive sublattice, is straightforward, but that in R can be handled easily only if we ignore the dependence of M_R on X_R, that is, for $T\ll T_c$ [see Eq. (14)]. For anisotropy on both sublattices or for anisotropic interaction, no simple way to reduce to a one-sublattice problem has been found.

In the YbIG, the origin of the anisotropy is anisotropic exchange coupling; no one-sublattice model is really correct. But for small H (compared to exchange) F and R are forced to be almost antiparallel so either (or both) appears to seek the directions of maximum exchange coupling, the eight [111]'s. The particular way in which anisotropy is applied should not matter for small H. At intermediate fields ($H\approx H_{exchange}$) we find our results are qualitatively consistent with anisotropy in R only. This is, R strongly seeks [111]'s, and F then behaves as if it were isotropically coupled to R.[29] The very-high-field case, where F and R are

almost parallel, defies all simple reasoning,[30] but then the exchange minimum dominates to the extent that anisotropy does not much matter. Thus, the R-anisotropy model has a considerable region of usefulness.

In what follows, we will assume that transitions occur as the R sublattice tries to make the best compromise between its exchange minimum and the anisotropy wells. We will deal extensively with approximate forms of the free energy which are polynomials in the order parameter, and our results parallel many of those discussed in the general treatment of Landau and Lifshitz.[25] It is important to note, however, that for YbIG, at least, the analyticity of the free energy as function of the order parameter θ_F is not an *a priori* assumption, as in general treatment, but is a direct consequence of the known and physically well justified form of the free energy explicitly displayed in Eq. (2). Analyticity in θ_R is not obvious. But, since the calculations can always be done (and were, for the six-sublattice model, done) with θ_F as the order parameter (see Sec. II), statements regarding singularities in the YbIG examples retain their special claim to validity.

B. Classification of Phase Transitions

We discuss four types of phase transitions.

1. *Ordinary First Order*

These transitions require no special symmetry of the applied-field direction. The nature of the transitions is easiest to understand for small H. Then the exchange minimum is very shallow so it does not move R very much from some crystal easy direction, but it will make the well whose X_R is closest to $X_R^{\rm iso}$ the lowest minimum. There will, however, be locally stable solutions near all wells. In the neighborhood of $T_{\rm comp}$, the compensation point, the exchange minimum sweeps over all declinations (see Figs. 16 and 17), so that all wells are successively favored. For YbIG, eight phases are represented near $T_{\rm comp} = 5.92\,^\circ$K. The sublattices jump between wells when $X_R^{\rm iso}$ is about half way between the X_R's giving the well locations. The jumps are discontinuous, so these transitions are first order – they involve hysteresis and have latent heats (save for $H = 0$), and magnetic moment discontinuities.

As an example, consider the transition in YbIG between [111] and [11 – 1] wells when the applied field is along [001]. The midway point between wells is given by $X_R(H, T) = 0$, and this should give the phase boundary. From Fig. 17, we can see that the boundary should start vertically and curve toward higher temperature as the field is raised (see Fig. 21 for actual results).

The slope of first-order phase boundaries is subject to the Claussius–Clapeyron-type relation

$$\left.\frac{dH}{dT}\right|_{\rm coex} = -\frac{\Delta S}{\Delta M} \quad , \tag{22}$$

where Δ refers to changes between phases. Since a temperature increase at constant H always leads to a phase of higher entropy, and a field increase to higher moment, we find that if the phase boundaries have positive slope, as is most common, the low-temperature phase has the higher moment.

An example of the behavior of S, M, C, and χ at such a typical first-order transition is shown in Fig. 18(I). All these properties are discontinuous, although coincidentally the changes in C and χ are quite small. The conditions are $H = 90$ kOe along [111], $T = 10.17\,^\circ$K (point A in Fig. 20).

2. *Liquid-Vapor-Like Second Order*

Second-order phase transitions[31] can occur when an eigenvalue of the curvature tensor of the free energy vanishes simultaneously with the corresponding component of the gradient of the curvature. (There also must be no lower minima at remote places on the free-energy surface.) These two conditions can generally be satisfied at isolated points in the H-T plane. Physically, these points occur as we follow first-order transitions between neighboring wells toward higher fields. As the exchange minimum deepens it can effectively eliminate the double minima between wells and eventually sweep the sublattice continuously between them.

A liquid-vapor-like second-order point occurs in YbIG for $H = 43\,640$ kOe along [100], $T = 7.51\,^\circ$K (point B, Fig. 21). Note that although H is along a symmetry direction in this example, it need not be for this kind of transition to occur. Properties are illustrated in Fig. 18 (II). The specific heat, magnetic moment, and susceptibility present a rather remarkable aspect. The following phenomenological description explains all features very well.

For H along [100], the free energy (ignoring the R sublattice susceptibility) can be approximated by

$$F = A(X_R^2 - \tfrac{1}{3})^2 + \tfrac{1}{2}(H^2 M_R^2/\lambda M_F^2)(X_R - X_R^{\rm iso})^2 \quad , \tag{23}$$

where we are now treating X_R as the order parameter and the exchange minimum has been approximated by its second-order Taylor expansion about $X_R^{\rm iso}$ [which is given in turn by Eq. (12)].

We next define

$$p \equiv H^2 M_R^2/4A\lambda M - \tfrac{1}{3} \quad , \tag{24}$$

$$q \equiv -\frac{H^2 M_R^2}{4A\lambda M_F^2}\left(\frac{H^2 + \lambda^2 M_R^2 - \lambda^2 M_F^2}{2\lambda H M_R}\right) \quad ,$$

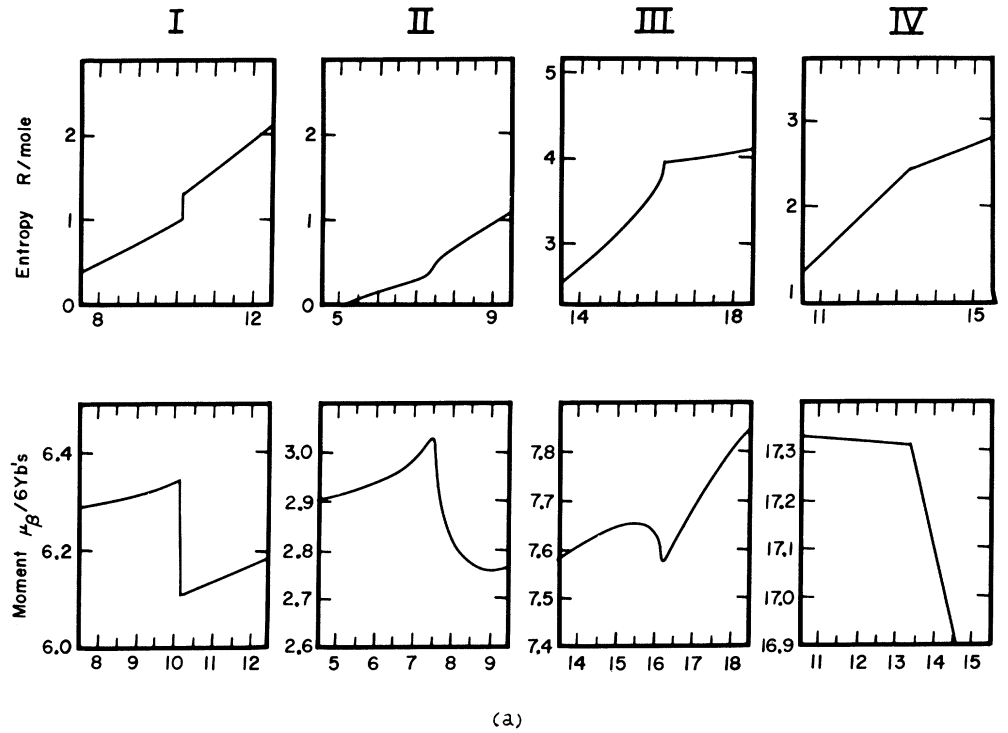

(a)

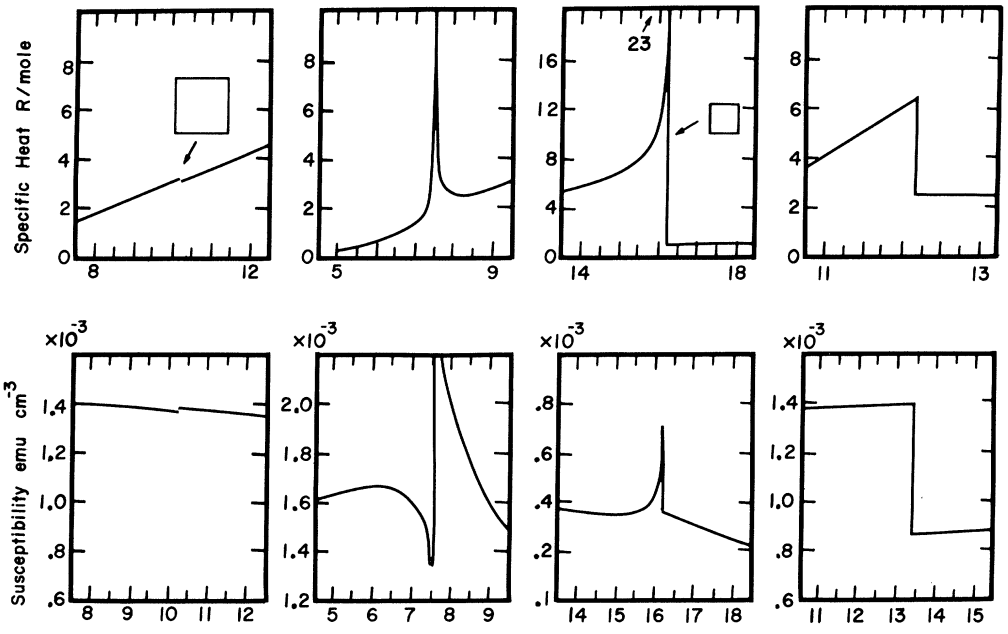

(b)

FIG. 18. S, M, C, and χ at four types of phase transitions in (anisotropic) YbIG: (I) first-order – all discontinuous (area on C plot gives latent heat); (II) liquid-vapor-like second order – S and M continuous, C and χ diverge; (III) symmetry-affected first order – all properties discontinuous with rapid changes *preceding* the transition; (IV) symmetry-affected second order – S and M continuous, C and χ finite but discontinuous.

so that F may be simply rewritten as

$$F = 4A\,(\tfrac{1}{4}X_R^4 + \tfrac{1}{2}pX_R^2 + qX_R) + \text{const.} \tag{25}$$

The equation of state for X_R is

$$X_R^3 + pX_R + q = 0\ . \tag{26}$$

This is a particularly simple form of a van der Waals equation and it solutions have the properties familiar from van der Waal's theory of condensation: $p>0$, one real root which has the sign opposite to that of q; $p<0$, three real roots (for small q), two stable first-order transitions between them when q changes sign; $p=0$, critical point at $q=0$. The coexistence curve in H-T is given by $q(H, T) = 0$. Let us define

$$\begin{aligned} &H_c = \sqrt{(\tfrac{4}{3}A\lambda)}, \quad h = H - H_c\,, \\ &\overline{T}_c \text{ such that } H_c^2 + \lambda \overline{M}_R^2(\overline{T}_c) - \lambda M_F^2 = 0, \quad t = T - \overline{T}_c\,, \\ &a = [\overline{M}_R(\overline{T}_c) - M_R(\overline{T}_c + t)]/t\ , \end{aligned} \tag{27}$$

where, in particular, H_c and T_c are the critical field and temperature, respectively.

We now derive the functional forms of p and q near the critical point for H along [100] in YbIG. We have ($\pm 30\%$)

$$A = 2\times 10^6 \text{ erg cm}^{-3} \tag{28a}$$

(from numerical results on variations of the free energy with Fe sublattice direction at $T = 7\,^\circ$K and $H = 0$),

$$a = 4 \text{ emu } {}^\circ\text{K}^{-1} \tag{28b}$$

(from numerical results on the variation of M_R near, but not including, the critical region averaged over locally stable states).

Also, from Eq. (20), we note that M_R may be taken equal to M_F except when they occur in differences. The simplified forms for p and q are

$$\begin{aligned} p &= \tfrac{2}{3}[h/H_c - (a/M_F)t]\ , \\ q &= \tfrac{1}{3}[(\lambda a/H_c)t - h/\lambda M_F]\ . \end{aligned} \tag{29}$$

Clearly, the critical point occurs at $h = t = 0$. The slope of the coexistence curve ($q = 0$) is about 10^4 Oe/deg (compare B in Fig. 21). We will work out the properties as we approach the critical point along $p = 0$ or $h/t = 8\times 10^2$ Oe/deg. This path has a small slope and should closely approximate results for $h/t = 0$ appropriate to Fig. 18. We find then that[32]

$$X_R = -(\lambda a/3H_c)^{1/3}t^{1/3} \approx -0.3\,t^{1/3}\ . \tag{30}$$

The entropy and specific heat are derived by total differentiation of F in the same manner as for the isotropic case [see Table II and also Eqs. (3) and (5)]:

$$S - S_0 = 4A\left(\frac{X_R^2}{2}\frac{\partial}{\partial t}p + X_R\frac{\partial}{\partial t}q\right) = \frac{4Ad}{3M_F}\left(X_R^2 - \frac{\lambda M_F}{H_c}X_R\right), \tag{31}$$

$$C - C_0 = -4AT\left(X_R\frac{\partial}{\partial t}p + \frac{\partial}{\partial t}q\right)\frac{\partial X_R}{\partial t}\ , \tag{32}$$

where S_0 and C_0 give a nontransition background. By differentiating (26), we find

$$\frac{\partial X_R}{\partial t} = \left(X_R\frac{\partial p}{\partial t} + \frac{\partial}{\partial t}q\right)\Big/3X_R^2\ . \tag{33}$$

Thus,

$$C - C_0 = (4ATa^2/9M_F^2)[\lambda M_F/H_c - 2X_R]^2/3X_R^2\ . \tag{34}$$

The values of Eq. (28) imply that $\lambda M_F/H_c$ is about 4, so in the possible range of X_R, and especially for $-\sqrt{\tfrac{1}{3}} < X_R < \sqrt{\tfrac{1}{3}}$, the numerator is almost constant. C, thus, diverges near $X_R = 0$ as X_R^{-2} or $t^{-2/3}$.

The magnetic moment and susceptibility are derived similarly by differentiation, this time with respect to h:

$$\begin{aligned} M - M_0 &= -4A\left(\frac{X_R^2}{2}\frac{\partial p}{\partial h} + X_R\frac{\partial q}{\partial h}\right) \\ &= -\frac{4A}{3\lambda M_F}\left(\frac{\lambda M_F X_R^2}{H_c} - X_R\right), \end{aligned} \tag{35}$$

$$\begin{aligned} \chi - \chi_0 &= 4A\left(X_R\frac{\partial p}{\partial h} + \frac{\partial q}{\partial h}\right)^2\Big/3X_R^2 \\ &= \frac{4A}{9\lambda^2 M_F^2}\left(\frac{2\lambda M_F}{H_c}X_R - 1\right)^2\Big/3X_R^2\ . \end{aligned} \tag{36}$$

These results are similar to those in (31) and (34), except that the large factor $\lambda M_F/H_c$ appears multiplying $2X_R$ rather than 1 in the numerator of χ and analogously for M. Thus, the transition part of χ, after rising, drops to zero for $X_R = \frac{1}{8}$, well within the range of interest. From (30) this event is expected to occur 0.07 °K below the transition, in good agreement with results in Fig. 18(II). At higher temperatures, up through and above the transition, χ has the expected $t^{-2/3}$ behavior. Similarly, the maximum in M below the transition is explained by Eq. (35). The good agreement of this phenomenological approach with the numerical results may seem surprising, but it merely reflects the insensitivity of the nature of the transition to details of origins of the anisotropy.

The above-described first-order lines ending in liquid-vapor-like critical points exhaust the transition types for applied field in a general direction. When there is a symmetry of applied-field direction, qualitatively different "symmetry-affected"

transitions can occur. We next discuss two of these, a first-order line whose special properties derive from threefold rotation symmetry about [111], and a second-order line deriving from twofold rotations about [100].

3. Symmetry-Affected First Order

The transition at point C {($H = 110$ kOe along [111], $T = 16.18\,^{\circ}$K (see Fig. 20)} is our example of a symmetry-affected first-order transition. The behavior of S, M, C, and χ is shown in Fig. 18(III). Below, we present a phenomenological theory showing how the major features of the transition are determined by symmetry.

When H is along [111], the expansion of F to fourth order in deviations of the F sublattice[33] from the direction of H takes the form

$$F = B[\tfrac{1}{2}\bar{p}(\theta^2+\phi^2) + \tfrac{1}{3}\bar{q}(\theta^3 - 3\theta\phi^2) + \tfrac{1}{3}\bar{r}(\phi^3 - 3\phi\theta^2) + \tfrac{1}{4}(\theta^2+\phi^2)^2] \ , \quad (37)$$

where θ gives deviation in the (110) plane and ϕ gives the out-of-plane displacement [i.e., in $(-1-12)$]. $B>0$ ensures local stability for some small deflection. No linear term is allowed by the threefold rotation symmetry, but third-order terms are allowed. This circumstance is the key to the phase-transition behavior.

Next, we take $\phi = 0$, implying that (110) is the easy plane. We then have

$$F = B\theta^2(\tfrac{1}{4}\theta^2 + \bar{q}\tfrac{1}{3}\theta + \tfrac{1}{2}\bar{p}) \ . \quad (38)$$

The $\bar{p}$ term comes mostly from the exchange minimum [see Eq. (19)]; $\bar{q}$ comes entirely from anisotropy {it can be gotten by transforming Eq. (21) so that X_R refers to H along [111]}.

The nature of the solutions to (38) follows by considering the parabola in the parentheses. Thus, if

$$\tfrac{1}{9}\bar{q}^2 - \tfrac{1}{2}\bar{p} < 0 \ ,$$

then $\theta = 0$ (aligned state) is lowest energy; if

$$\tfrac{1}{9}\bar{q}^2 - \tfrac{1}{2}\bar{p} > 0 \ ,$$

then for q small there are two minima, one +, one −; lowest energy has the opposite sign to $\bar{q}$ (first-order transition when $\bar{q}$ changes sign). The phase boundaries (see Fig. 20) are then given by

$$\bar{q}(H, T) = 0$$

["straight" boundary between $11-1$ and $-1-11$ phases (first-order transition with no change in symmetry)] and

$$\tfrac{1}{9}\bar{q}^2 = \tfrac{1}{2}\bar{p}$$

[outer "circular" boundary between canted $(11-1$ or $-1-11)$ and aligned phases (first-order transition which does change symmetry)]. The intersection of these boundaries occurs at $\bar{p} = \bar{q} = 0$ (point F), and only for paths which pass through this point is the canted-aligned phase transition of second order.[34]

For point C we take $\bar{q} \neq 0$, approximately constant, and guess the variation of $\bar{p}$ from Eq. (19). Writing $p = \alpha t$, we have for C (specific heat)

$$C = \tfrac{1}{2} B\alpha^2 T[\bar{q}/(\bar{q}^2 - 4\alpha t)^{1/2} + 1] \ , \quad (39)$$

where $t = T - T_0$ (T_0 is defined as the vanishing temperature for p at our constant field of 110 kOe). Letting $H \sim \lambda M_F$ and $T \sim T_c$, we have from Eq. (19)

$$\alpha = 3/T_c \ , \quad B\alpha T = \lambda M_F^2 \ , \quad T_c = \lambda M_F^2/R \ , \quad (40)$$

where R is the gas constant (per cubic cm of material to be here consistent).

C would diverge at $4\alpha t = \bar{q}^2$ save for the fact that a first-order transition intervenes at $4\alpha t = \frac{8}{9}\bar{q}^2$, that is at $\frac{1}{2}p = \frac{1}{9}\bar{q}^2$. (In the isotropic system the transition would occur earlier still at $t = 0$.) The largest value achieved by C is thus

$$C_{\max} = (3\lambda M_F^2/2T_c)[3+1] = 9(3+1)R/\text{mole} \ , \quad (41)$$

where the first number in the sum is the contribution due to the special nature of the transition and the second corresponds to the maximum specific heat before the second-order transition in the isotropic ferrimagnet. $C_{\max}$ is independent of the size of $\bar{q}$; however, the width and, hence, the entropy in the symmetry-affected portion vary as $\bar{q}^2$. The half-width of the symmetry part of C and the entropy discontinuity, respectively, are

$$\Delta t = \bar{q}^2/9\alpha \ \text{K}^{\circ}, \qquad \Delta S = \tfrac{4}{3}\bar{q}^2 R/\text{mole} \ . \quad (42)$$

After the transition, that is in the aligned state, the specific heat is relatively small and slowly varying.

To get some idea of the values of Δt and ΔS expected for YbIG we computed $\bar{q}$ for anisotropy of the form Eq. (21) with constants from Eq. (28). (This is an overestimate since partial demagnetization of the R sublattice, as well as the fact that the anisotropy seems best keyed to X_R, both lessen the effect.) The result is that $\bar{q} = 0.4$, so that Δt would be about $10^{-1}\,^{\circ}$K and ΔS about $0.2R$/mole. Actually [see Fig. 18(III)] the width and the latent heat calculated for the six-sublattice model are about half this, so our rough (over-) estimate is not bad. Note that there is also an anomaly in the susceptibility which arises from the variation of $\bar{p}$ with applied field.

4. *Symmetry-Affected Second Order*

The last example is a transition on crossing a second-order transition line (Fig. 21, point D, H along [100] = 250 kOe, $T = 13.4\,^{\circ}$K). Second-order lines occur whenever there is a reflection symmetry in the constraint parameter. Obviously, the isotropic ferrimagnet canted-aligned transition is a special case. The canted-aligned transition is also second order for the fourfold symmetry afforded by H along [100]. An equation for the phase boundary is most easily gotten from Eq. (19) with an anisotropy term of the form in Eq. (21)[33]:

$$\lambda M_R H M_F / |\lambda M_F - H| - H M_F + \tfrac{8}{3} A = 0 \ . \qquad (43)$$

For high fields ($H \simeq 250$ kOe), we have the transition at

$$H = \lambda(M_R + M_F) + 4AM_R/3HM_F \ , \qquad (44)$$

where the last term represents a shift of the transition boundary toward a higher field by about 10 Oe compared to the isotropic case, $A = 0$. Unlike previous cases, this description is most unrealistic in detail, but the scale of the influence of the anisotropy is correct.

For low fields ($H \ll \lambda M_F$) we may (with some more confidence) approximate the condition for alignment as

$$H(M_F - M_R) = \tfrac{8}{3} A \ . \qquad (45)$$

Equation (45) describes, in particular, the behavior at high temperatures where the R-sublattice magnetic moment M_R is small compared to M_F and its contribution to the anisotropy $A(T)$ falls approximately as M_R, yielding the exponential tail on the phase boundary (see Fig. 21).

The behaviors of S, M, C, and χ are shown in Fig. 18 (IV). They exhibit the same qualitative features discussed for the isotropic case. It should be noted that here the second-order line depends crucially on the field direction for its existence; the phase transition will subside to merely a region of rapid sublattice adjustment as soon as there is any deviation from precise symmetry.

This completes our classification of phase transitions and accounts for all the types of behavior "discovered" in our numerical calculations on YbIG.

There might be other types of transitions in crystals of other than cubic symmetry, and even different cubic types which involve azimuthal instabilities coupled to changes in declination angle. These possibilities were not investigated in the present study except to note that such a transition does occur in YbIG for field along [110].

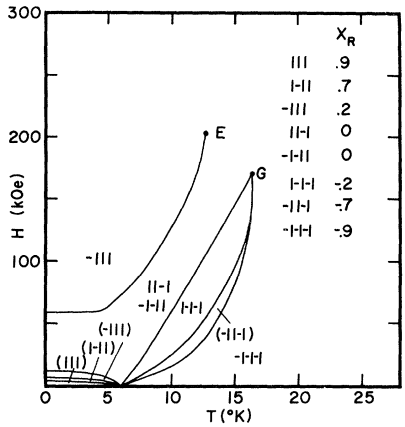

FIG. 19. Phase boundaries for H along [314]. X_R are the direction cosines of the source anisotropy wells (i.e., the local minima to which the R sublattice would return were H rapidly decreased to 0). Phases are labeled by the source-well indexes. The boundaries follow lines of the constant X_R^{iso} (see Fig. 17) which would place the exchange minimum about halfway between wells. Observe the [−111] to [11−1] phase boundary which by the above rule follows $X_r \sim -0.1$. This runs off to the left since $T = 0\,^{\circ}$K corresponds to M_R/M_F, equal to 1.01, and thus the swing toward higher M_R/M_F indicated in Fig. 17 cannot be followed. However, the line returns at still higher field. All lines are first order. Second-order points occur at E and G.

C. Phase Boundaries

Further clarification of when the above four kinds of transitions occur are provided by the following examples of H-T-plane phase boundaries. The cases are distinguished primarily by the symmetry of the applied-field direction.

A field along [314] (see Fig. 19) eliminates all symmetry from the cubic crystal; at low field there are eight phases deriving from the eight [111] easy directions of the R sublattice. Each phase is labeled by the "source" direction, i.e., that to which M_R would return if the field were removed and there were no jumping between wells. By chance, the [11−1] and [−1−11] directions both make the same angle to [314], so the derived phases are very close to degenerate; we take them to be degenerate for simplicity.

The boundaries behave as expected from R-sublattice anisotropy. That is, they follow fairly well lines of constant X_R^{iso} (exchange minimum) which are about halfway between the well X_R's (see Fig. 17). (Values of X_R, direction cosines of M_R to H, at the source anisotropy wells are listed in Fig. 19.) The boundaries diverge from the compensation point and approximately converge near $H = \lambda M_F$ at the "demagnetization temperature" of R. It is notable that there is no phase transition to a

completely aligned phase; without special symmetry the anisotropic ferrimagnet never aligns except by chance, and then only at isolated points in the H-T plane. This behavior is similar to that of other anisotropic magnets: Exact alignment can ordinarily be achieved only for field applied in principal anisotropy directions.

At higher field, the anisotropy wells become overwhelmed by the steep exchange minimum. However, the second-order points which mark the ends of the first-order lines are not often visible because they occur when two minima are driven together by the competing effects of anisotropy and exchange. While this takes place, some other more single-minded local minimum usually wins out. Thus, the $[-1-11]$ and $[-1-1-1]$ phases coalesce while $[1-1-1]$ is lowest. Only the critical point between $[-111]$ and $[11-1]$ (point E) occurs in a visible range. The point G must also be second order, but it has not been investigated in detail.

A field along [111] leaves a threefold symmetry axis and a reflection plane (which turns out to be the easy plane). There are four inequivalent phases (see Fig. 20). The [111] phase (R parallel to H) has a limited range of existence because the large halfway value of X_R between this and the $[11-1]$ well, $X_R \sim 0.7$, is achieved at quite small fields unless M_R is much larger than M_F. For $T = 0\ ^\circ\mathrm{K}$, $M_R/M_F = 1.01$, so the flip field as derived from Fig. 17 is 2.5 kOe (compare with the 1.53-kOe result from the six-sublattice numerical calculation, Fig. 20). The $[11-1]$ phase should go to $[-1-11]$ at $X_R \sim 0.2$ and this also gives rather well the course of the computed phase boundary. Similarly, the transition to the antiparallel state

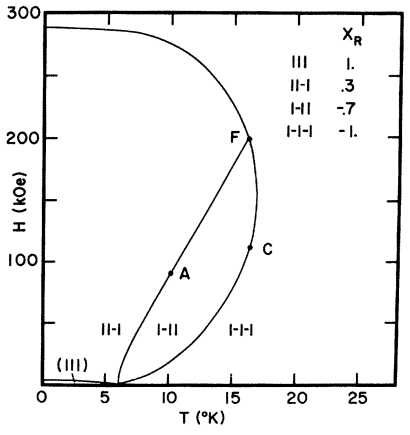

FIG. 20. Phase boundaries for H along [111]. All lines are first order with ordinary transitions for the line containing A, symmetry-affected ones for the line containing C. Point F is second order.

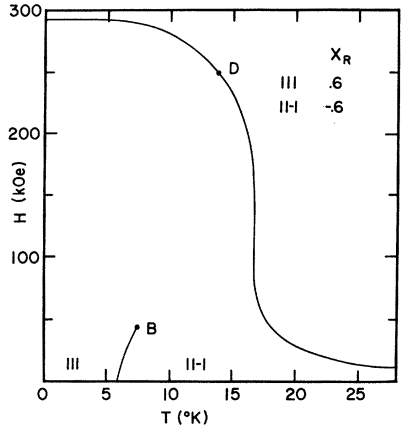

FIG. 21. Phase boundaries for H along [100]. The boundary ending at B (solid) is first order; B is a liquid-vapor-like second-order point. The outer boundary (dashed) separates canted and aligned phases and is second order.

$[-1-1-1]$ roughly follows $X_R \sim -0.8$. Note that in high field, although $X_R \sim +0.7$ reappears in realizable range of M_R/M_F (Fig. 3), there is no reoccurrence of a [111] phase in Fig. 20. This is because the exchange minimum is then so deep that distinction between the [111] and $[11-1]$ source wells is washed out. All transitions are first order except for the second-order point at F. The outer phase-boundary transition is symmetry affected.

Lastly, field along [001] (Fig. 21) leaves a fourfold axis and two reflection planes (110) and (100), of which (110) is always easy. There are two inequivalent wells. The first-order boundary between $[-1-1-1]$ and $[-1-11]$ phases follows $X_R \sim 0$ until it ends at point B. The outer phase boundary is to a totally aligned state; the symmetry ensures that it is second order and that it cannot end.

VI. CONCLUSION

We have presented theoretical results displaying four kinds of phase transitions which occur in the field-induced canted configurations of YbIG. Although our choice of parameters may not be a best fit to available data, the mean-field basis of the theory is very well justified and this lends considerable credibility to the predicted analytic behavior of singular thermodynamic functions near the phase transitions. We have also developed the phenomenological concepts of "exchange minima" and "anisotropy wells" which should be useful in describing any anisotropic ferrimagnet liable to a mean-field approach. These explain the course of phase boundaries in the H-T plane and also how phase-transition properties depend on the anisotropy, and the magnitude and symmetry of

direction of the applied field.

Measurements on single crystals in applied magnetic fields of 40–80 kOe could provide an accurate check on much of the predicted phase-transition behavior.

ACKNOWLEDGMENTS

The author would like to thank A. E. Clark for inspiring this work and for providing advice and unpublished experimental results during its progress. Thanks also are due R. G. Wheeler for helpful discussions, the National Science Foundation for making possible the computer calculations, and W. P. Wolf for suggestions regarding the manuscript.

---

*Work partially supported by the National Science Foundation.

[1]Not to be confused with zero-field noncollinearity as in "star" structures [B. Y. Boucher, R. Buhl, and M. Perrin, J. Appl. Phys. 38, 1109 (1967); Y. Yafet and C. Kittel, Phys. Rev. 87, 290 (1952)] or anisotropy-affected canting in weak ferromagnets and in rare-earth-iron garnets [S. Geller, J. H. Williams, G. P. Espinosa, and R. G. Sherwood, Bell System Tech. J. 43, 565 (1964); I. Nowik, J. Appl. Phys. 40, 5184 (1969)].

[2]L. Néel, Ann. Phys. (Paris) 3, 137 (1948).

[3]J. N. McElearney, H. Forstat, and P. T. Bailey, Phys. Rev. 181, 887 (1969).

[4]J. Kanamori, K. Motizuki, and K. Yosida, Buseiron Kenkyu 63, 28 (1953); J. Motizuki, J. Phys. Soc. Japan 14, 759 (1959).

[5]C. J. Gorter and T. van Peski-Tinbergen, Physica 22, 273 (1956).

[6]A. E. Clark and E. Callen, J. Appl. Phys. 39, 5972 (1968) (includes references to numerous other recent contributions).

[7]M. J. Besnus, G. Munschy, and A. J. P. Meyer, J. Appl. Phys. 39, 903 (1968).

[8]B. P. Goranskii and A. K. Zvezdin, Zh. Eksperim. i Teor. Fiz. Pis'ma v Redaktsiyu 10, 196 (1969) [Soviet Phys. JETP Letters 10, 124 (1969)].

[9]See, for example, M. T. Hutchings and W. P. Wolf, J. Chem. Phys. 41, 617 (1964).

[10]J. H. Van Vleck, Progr. Sci. Tech. Rare Earths 2, 1 (1966).

[11]The second-order exchange Zeeman effect is expected (Ref. 15) to give an added amount of $0.3\beta/6$ Yb's. This is quite small compared to our uncertainty in the primary Zeeman effect (g factors) and will not be treated explicitly.

[12]K. A. Wickersheim, Phys. Rev. 122, 1376 (1961); K. A. Wickersheim and R. L. White, Phys. Rev. Letters 8, 483 (1962); A. J. Seivers and M. Tinkham, Phys. Rev. 124, 321 (1961); 129, 1995 (1963).

[13]S. Geller, J. P. Remeika, R. C. Sherwood, H. J. Williams, and G. P. Espinosa [Phys. Rev. 137, A1034 (1965)] did not find any residual moment at $T=0$ °K. R. Pauthenet [Ann. Chim. Phys. 3, 424 (1958)] found the Yb moment exceeded the Fe by 0.5β. The Wickersheim parameters give a compensation point 5.92 °K.

[14]We do not mean to imply that the parameters in Table I are the most accurate available or that they constitute a best over-all fit. We concentrate on fitting the compensation point, since this determines much of the qualitative behavior. The slightly revised parameters of Wickersheim and White (Ref. 11) do not give a compensation point ($T=0$ °K, Yb moment $=9.948\beta/6$ Yb's). Wolf's choice for parameters (Ref. 15) just barely gives one (Yb moment $=10.02$).

[15]W. P. Wolf, M. Ball, M. T. Hutchings, M. J. M. Leask, and A. F. G. Wyatt, J. Phys. Soc. Japan Suppl. 17, 443 (1962).

[16]G. P. Rodrigue, H. Meyer, and R. V. Jones, J. Appl. Phys. 31, 3765 (1960).

[17]Near the high-field phase boundary between aligned and canted phases for field applied in [111] (see Fig. 20) the anisotropy with respect to aximuthal variation of the Fe sublattice angle becomes unworkably small – so the easy plane, for this limited region, could not be identified. One further note – (110) is not always an easy plane for direction of field other than [111] and [100]. For example, with the field along [110] the moment often lied near the (–112) plane (not a symmetry plane).

[18]A. E. Clark and R. Alben, J. Appl. Phys. 41, 1195 (1970).

[19]A. E. Clark and T. R. McGuire (private communication).

[20]Experimental results are by A. E. Clark reported in Ref. 6.

[21]These specific-heat results should be and, apparently, are identical to those previously calculated by J. W. Henderson and R. L. White, Phys. Rev. 123, 1627 (1961).

[22]J. H. Schelleng and A. E. Clark, Phys. Letters 29A, 172 (1969).

[23]R. F. Pearson, Proc. Phys. Soc. (London) 86, 1055 (1965); R. F. Pearson and K. Tweedale, J. Appl. Phys. 35, 1061 (1964); R. F. Pearson, *ibid.* 33, 1236 (1962).

[24]R. A. Buchanan and A. E. Clark, Solid State Commun. 7, 1087 (1969).

[25]L. D. Landau and E. M. Lifshitz, *Statistical Physics* (Addison-Wesley, Reading, Mass., 1958), Chap. 14.

[26]J. S. Smart, *Effective Field Theories of Magnetism* (Saunders, New York, 1966), pp. 6, 29.

[27]$\overline{F}(T)$ is taken here, as in all our calculations, so as to reproduce the lattice specific heat of LuIG as reported by Harris and Meyer (Ref. 11): $\overline{F}(T)=0.564\times10^{-5}T^4$ cm^{-1}/6 Yb, $\overline{S}=3.25\times10^{-5}T^3R$/mole.

[28]In terms of cubic sublattice anisotropy constants $A=-\frac{3}{4}K_1-\frac{1}{2}K_2$.

[29]This is not obvious from the physics, but it has been verified by examining relationships between sublattice angles in the numerically solved cases.

[30]When F and R are parallel, the exchange opposes the dominant applied field and it might be thought that the sublattices would prefer [100] a weak exchange direction, and, incidentally, a somewhat higher moment direction as well. But at 300 kOe, [111] is still the easiest direc-

tion for the crystal. The explanation is hidden in the complex compromises made by each of the six R sites, none of which generally has its moment fully aligned, even when the sum of the moments is aligned.

[31]R. Alben, Phys. Rev. Letters 24, 68 (1970); another mention of this kind of point occurs in Ref. 5, but in the case treated there, the mean-field approach is not as well justified as for YbIG.

[32]Near (H_c, T_c) X_F behaves as $q^{1/3}$ for all paths except the coexistence curve $(q=0)$. Along $q=0$, X_F behaves as $p^{1/2}$. It is traditional to denote by δ the exponent which gives the behavior of the forcing variable as a function of the state variable: $t=aX^{\delta}$. The value of δ is 3 for this classical critical point. The variation of X along the coexistence curve is given by the exponent β and here $\beta=\frac{1}{2}$, again the classical value.

[33]For the high temperature here the R-sublattice model of anisotropy is difficult to justify since R is almost demagnetized. Thus, unlike in previous treatments, we here use the F-sublattice model.

[34]However, since there is a change in symmetry the "outer" phase boundary cannot end, it continues as a first-order line. The point F exhibits behavior similar to a second-order line (point D) and not like a liquid-vapor-like point (B).

PHYSICAL REVIEW B VOLUME 2, NUMBER 7 1 OCTOBER 1970

Nuclear Quadrupole Spin-Lattice Relaxation and Critical Dynamics of Ferroelectric Crystals

G. Bonera, F. Borsa, and A. Rigamonti
Istituto di Fisica dell'Università di Pavia,
Gruppo Nazionale di Struttura della Materia del Consiglio Nazionale delle Ricerche, Pavia, Italy 27100

(Received 21 January 1970)

The effect on the nuclear spin-lattice relaxation of the anomalous temperature dependence of generalized unstable lattice modes near the ferroelectric transition is investigated both theoretically and experimentally. Expressions for the relaxation rate near T_c are derived for typical cases of critical dynamics of ferroelectric crystals. For the case of undamped soft-phonon modes it is shown that, on the basis of a Raman two-phonon relaxation mechanism, the relaxation rate should behave near the transition temperature as $(T-T_0)^{-n}$, where n depends on the shape of the dispersion curve of the soft branch. On the other hand, for the case of damped-oscillatory modes or diffusive modes, the relaxation rate, derived by using the classical approach for the direct relaxation process, should behave as $(T-T_0)^{-1/2}$ or as $\ln(T-T_0)$ if the anisotropic character of the dipolar interaction is taken into account. An experimental investigation of the nuclear spin-lattice relaxation rate in $NaNO_2$ single crystal is presented. The resonance spectrum and the recovery law under different conditions are discussed. The results of the relaxation rate as a function of temperature, angular orientation, and resonance frequency indicate the existence of a damped generalized soft mode or critical diffusive mode. The available data on the shape of the relaxation-rate peak tends to favor the logarithmic singularity, in agreement with the prediction of an anisotropic interaction. From the analysis of the data, it is inferred that the soft mode can be identified as the flipping motion along the ferroelectric c axis of the electric dipoles associated with the NO_2^- group, which seem to be mainly correlated along the a axis. The relaxation measurements support the recent suggestion for a new low-temperature phase transition.

I. INTRODUCTION

Nuclear magnetic resonance (NMR) techniques have been widely employed in order to gain information on the phase transition and on the properties of ferroelectric crystals.[1] Information on structural or symmetry changes occurring at the phase transition can be obtained from the splitting and/or shift of the NMR spectrum associated with the static quadrupole interaction with the lattice. Furthermore from the temperature dependence of the quadrupole interaction one can deduce the temperature dependence of the spontaneous polarization. The temperature dependence of the jumping frequency of atoms between sites with different electric-field gradients (efg) can be evidenced by the collapsing of the corresponding resonance lines. Finally, measurements of spin-lattice relaxation time governed by magnetic dipolar interactions and quadrupole interactions have been performed, mainly in hydrogen-bonded ferroelectrics, in order to study the proton or deuteron motion both in the paraelectric and ferroelectric phases.

In ordinary diamagnetic nonconducting ferroelectrics the main source of relaxation for nuclei with $I>\frac{1}{2}$ is the coupling between the nuclear-spin system and the crystal lattice through the interaction